Comput Mech (2015) 56:1039–1054
DOI 10.1007/s00466-015-1217-3

ORIGINAL PAPER

A strain-morphed nonlocal meshfree method for the regularized particle simulation of elastic-damage induced strain localization problems

C. T. Wu[1] · Youcai Wu[2] · M. Koishi[3]

Received: 11 August 2015 / Accepted: 1 November 2015 / Published online: 13 November 2015

Abstract In this work, a strain-morphed nonlocal meshfree method is developed to overcome the computational challenges for the simulation of elastic-damage induced strain localization problem when the spatial domain integration is performed based on the background cells and Gaussian quadrature rule. The new method is established by introducing the decomposed strain fields from a meshfree strain smoothing to the penalized variational formulation. While the stabilization strain field circumvents the onerous zero-energy modes inherent in the direct nodal integration scheme, the regularization strain field aims to avoid the pathological localization of deformation in Galerkin meshfree solution using the weak-discontinuity approach. A strain morphing algorithm is introduced to couple the locality and non-locality of the decomposed strain approximations such that the continuity condition in the coupled strain field is met under the Galerkin meshfree framework using the direct nodal integration scheme. Three numerical benchmarks are examined to demonstrate the effectiveness and accuracy of the proposed method for the regularization of elastic-damage induced strain localization problems.

Keywords Meshfree · Nodal integration · Nonlocal · Stabilization · Regularization

✉ C. T. Wu
ctwu@lstc.com

[1] Livermore Software Technology Corporation, Livermore, VA 94550, USA

[2] Karagozian & Case, 700 N Brand Blvd, Suite 700, Glendale, CA 91203, USA

[3] Koishi Laboratory, The Yokohama Rubber Co., Ltd., Hiratsuka, Kanagawa 254-8601, Japan

1 Introduction

Meshfree or particle methods [7,11,19–21] are attractive in various industrial applications involving high gradients, large deformation and moving discontinuities. Three types of instabilities [5] arise when a solid mechanics problem is solved by the meshfree nodal integration method. Spurious energy mode in deformation is the first type of instabilities which mainly emanates from the rank instability [3] of the meshfree discrete system. The rank instability is caused by the under-integration of weak forms inherent in the central difference formula from the direct nodal integration scheme, and it requires numerical stabilization. Strain localization [18] is driven by the material instability which presents the second type of instability in meshfree nodal integration method. Physically, it is recognized [15,16] that the onset of strain localization in the rate-independent material coincides with the loss of ellipticity of the incremental problem. Mathematically, the strain localization leads to the ill-posedness of the incremental boundary value problem and requires a localization limiter [17]. Tension instability [13] is the third meshfree instability from discretization which results from the interaction of the second derivative of Eulerian kernel and the tensile stress [5]. Nowadays, the tensile instability can be entirely cured by an employment of Lagrangian kernels [7,24] in the solid mechanics applications.

So far, several stabilization techniques have been developed to remove the spurious energy modes in the meshfree nodal integration solution. The meshfree Galerkin/least-squares (GLS) stabilization approach [3] presents a reconstructed weak form where a bilinear term consisting of the residual of equilibrium equation is employed to stabilize the solution. The principle drawback of this residual stabilization approach is the contradictory demands on the stabilization control parameter placed by accuracy requirement. In 2001,

Chen et al. [9] developed a Stabilized Conforming Nodal Integration (SCNI) method in which the "integration constraint" concept was proposed for the design of an accurate meshfree nodal integration algorithm. Based on the integration constraint, a strain-smoothing scheme was introduced as a stabilization process for nodal integration. Various applications [28,38,39] of SCNI method have studied in structural and solid mechanics problems. The consistency conditions for arbitrary order exactness in the Galerkin approximation were introduced by Chen et al. [11,14] to further reduce the solution errors of PDEs from quadrature inaccuracy. Recently, Wu et al. [35] developed the Smoothed Particle Galerkin (SPG) method in which a smoothed displacement field is introduced to stabilize the meshfree Galerkin nodal integration solution in large deformation and damage analyses. Most recently, the displacement smoothing technique in SPG method also has been adopted in the state-based peridynamics [25] and the SCNI method [9] for the material damage analyses [36]. It was shown [37] that SPG method is closely related to the nonlocal meshfree method [8] by means of strain regularization analysis. Their analysis results reveal the SPG method is developed based on a fully nonlocal model in strain approximation. In other words, the local and nonlocal strain fields are not decoupled in the SPG method. In order to restore the locality of SPG strain approximation for the inhomogeneous deformation in non-failure analyses, Wu et al. [37] has developed a strain gradient stabilization (SGS) scheme. In SGS scheme, the first-order strain gradients are derived based on the decomposed strain field from the displacement smoothing to provide the necessary stabilization effect in the meshfree nodal integration method. The SGS scheme excludes the second and higher-order strain gradients for non-failure analysis leading to a penalty formulation with the penalty (stabilization) parameter coming naturally from the first-order strain gradients solely for stabilization. A unique property of the resultant SGS formulation is it does not require the background cells for the domain integration. Other meshfree stabilization approaches [38] are often based on the fully nonlocal model in strain approximation and cannot preclude the use of background cells for integration, therefore, pose certain challenges in both programming and simulating using the Galerkin meshfree methods.

Similar to the damage-induced mesh sensitivity [2] in finite element method, the discretization in Galerkin meshfree method rules the size of the strain localization zone. Numerically, the discretization sensitivity in strain localization problem is a consequence of shortcomings of the underlying mathematical modeling [23]. To avoid this pathological localization of deformation in Galerkin meshfree method, several meshfree regularization techniques have been developed. Based on the concept of nonlocal damage and gradient-enhanced damage modeling techniques [2,8] have developed a meshfree strain smoothing procedure to remedy the discretization sensitivity in damage-induced strain localization problem. The relationship between the integral-type and gradient-type nonlocal damage models [2] at the discrete level was established under their meshfree regularization framework [8]. Subsequently, the meshfree regularization procedure was applied to the SCNI method [9] by Wang and Li [29] in which a nodal-integrated smoothed strain field was introduced to enhance the accuracy as well as the efficiency in the regularized Galerkin meshfree method. Both elastic-damage analysis [29,30] and elasto-plastic damage analysis [38] have been conducted using this nodal-integrated regularized Galerkin meshfree method in explicit dynamics simulation. Nevertheless, an implementation of those meshfree regularization procedures still demands the background cells as an instance of the ones in meshfree stabilization procedures. Similar to the SPG method [35], those meshfree regularization methods were developed based on the fully nonlocal damage modeling technique where the higher-order strain gradients are contained in the strain approximations for the entire domain.

Stabilization and regularization are two important ingredients for an accurate particle simulation of damage-induced strain localization problems. The difficulties in obtaining a stable and regularized meshfree solution have prompted numerous techniques that aim to improve onerous stability issue in the nodal integration scheme and circumvent the discretization sensitivity in strain localization problems in the right place at the right time. The main goal of this paper is to introduce a strain-morphed meshfree method using the direct nodal integrated scheme for the analysis of elastic-damage induced strain localization problems with provided stabilization and regularization effects.

Our paper is organized as follows. In the next section, an overview on the nonlocal damage model is given. In Sect. 3, a strain-morphed meshfree method for providing the stabilization and regularization effects based on a decomposed smoothed strain field is derived. The corresponding variational formulation and discrete equations are given in Sect. 4. Three numerical examples are presented in Sect. 5 to illustrate the robustness and accuracy of the proposed method. Section 6 concludes with a brief summary.

2 Overview on damage model and existing non-local strain approaches

The basis for damage model is the introduction of a local damage variable impacting the stiffness of the material. As a prototype of a softening continuum, we consider the scalar isotropic elastic-damage model described by the stress–strain relationship [1]

$$\boldsymbol{\sigma} = (1 - d)\, \boldsymbol{C} : \boldsymbol{\varepsilon} \tag{1}$$

with damage law defined in total form

$$d = g(\boldsymbol{\kappa}) \tag{2}$$

and Kuhn–Tucker loading-unloading conditions given by

$$f(\boldsymbol{\varepsilon}, \boldsymbol{\kappa}) \equiv \varepsilon_{eq}(\boldsymbol{\varepsilon}) - \boldsymbol{\kappa} \leq 0,\ \dot{\boldsymbol{\kappa}} \geq 0,\ f(\boldsymbol{\varepsilon}, \boldsymbol{\kappa})\dot{\boldsymbol{\kappa}} = 0 \tag{3}$$

where $\boldsymbol{\varepsilon}$ is the strain tensor, $\boldsymbol{\sigma}$ is the Cauchy stress tensor, d is the damage variable and $\boldsymbol{C}$ is the fourth-order elasticity tensor. Function g is the damage evolution function which is a continuous function and designed such that $d = 0$ for the internal variable $\boldsymbol{\kappa}$ below a certain threshold, $\boldsymbol{\kappa}^0$. A simple equivalent strain $\boldsymbol{\varepsilon}_{eq}$ can be defined [2] as:

$$\varepsilon_{eq} = \sqrt{\frac{1}{E}\boldsymbol{\varepsilon} : \boldsymbol{C} : \boldsymbol{\varepsilon}} \tag{4}$$

where E denotes the Young's modulus.

The implementation of above elastic-damage model causes the pathological localization of deformation in finite element method as well as in Galerkin meshfree method [8]. As a result, the damage concentrates in a band of width depending on the size of nodal spacing in meshfree discretization, and the meshfree solution does not converge as the discretization model is continuously refined.

A number of nonlocal approaches have been proposed to regularize the soften media and control the localization phenomenon of the underlying continuum theory. One of the early approaches is to introduce an integral-type of nonlocal strain [2] into the local damage model. In this integral-type damage model, the growth of damage in a material point $\mathbf{x}$ is governed by a nonlocal equivalent strain $\bar{\varepsilon}_{eq}$ which is defined by

$$\bar{\varepsilon}_{eq}(\mathbf{x}) = \int_{\Omega} \Psi^b(\mathbf{x} - \boldsymbol{\xi})\, \varepsilon_{eq}(\boldsymbol{\xi})\, d\Omega \tag{5}$$

where $\Psi^b(\mathbf{x} - \boldsymbol{\xi})$ is the non-negative smoothing function of the distance $\|\mathbf{x} - \boldsymbol{\xi}\|$ and the subscript b denotes the radius of support in the strain smoothing function. With this nonlocal equivalent strain measure, the corresponding loading condition in Eq. (3) becomes

$$f(\bar{\boldsymbol{\varepsilon}}, \boldsymbol{\kappa}) \equiv \bar{\varepsilon}_{eq}(\boldsymbol{\varepsilon}) - \boldsymbol{\kappa} \leq 0 \tag{6}$$

The numerical advantage of this approach is that the kinematic and equilibrium equation remain standard. However in finite element implementation, the resulting stiffness matrices cannot be assembled by a conventional single element loop in Gauss points due to the expression of nonlocal strains in Eq. (5). In Galerkin meshfree method, more implementation challenges arise when the double integration loop based on background cells is used for the nonlocal stiffness matrices assembly.

An approach to avoid the double element loop in stiffness matrices assembly is the use of gradient-type of nonlocal strain [12]. In Galerkin meshfree method [8], the generation of strain gradient was controlled by the gradient reproducing conditions in reproducing kernel (RK) [22] approximation. This approach leads to a nonlocal strain field defined by [10]

$$\bar{\boldsymbol{\varepsilon}}(\mathbf{x}) = \boldsymbol{\varepsilon}(\mathbf{x}) + \sum_{i+j=1}^{n} \alpha_{ij} D_{ij} \boldsymbol{\varepsilon}(\mathbf{x}) \tag{7}$$

where $D_{ij}(\cdot) = \partial^{i+j}(\cdot)/\partial x_1^i \partial x_2^j$ is the standard differential operator, and α_{ij} is the corresponding coefficient of the strain gradient. As a consequence, the nonlocal equivalent strain is expressed in terms of nonlocal strain and given by

$$\bar{\boldsymbol{\varepsilon}}_{eq} = \sqrt{\frac{1}{E}\bar{\boldsymbol{\varepsilon}} : C : \bar{\boldsymbol{\varepsilon}}} \tag{8}$$

In [8] the nonlocal strain field $\bar{\boldsymbol{\varepsilon}}(\mathbf{x})$ is also introduced to the Galerkin approximation of the weak form solution through an assumed strain method [26]. The attendant meshfree regularization approach reduces programing complexity since it avoids the double integration loop in stiffness matrices assembly. On the other hand, this approach introduces a different type of complexity into the programing. Because Eq. (7) is evaluated at the Gauss points using the background cells approach [8], another set of discrete points based on the collection of Gauss points is needed for the RK approximation in the nonlocal strain computation. Additionally, the rendered nonlocal strain field is not only imposed on the damage zone but also the rest of undamaged domain.

3 A strain-morphed nonlocal damage model

The general form of smoothed strain field in meshfree method is defined by [8]

$$\bar{\boldsymbol{\varepsilon}}^b(\mathbf{x}) = \boldsymbol{\Theta}\boldsymbol{\varepsilon}(\mathbf{x}) \overset{def.}{=} \int_{\Omega} \tilde{\Psi}^b(\mathbf{x}; \mathbf{x} - \boldsymbol{\xi})\, \boldsymbol{\varepsilon}(\boldsymbol{\xi})\, d\Omega,\ \mathbf{x} \in \Omega \subseteq R^2 \tag{9}$$

where $\boldsymbol{\Theta} : L^2(\Omega) \to L^2(\Omega)$ denotes a L_2 projection operator, $\boldsymbol{\xi}$ denotes the position of the infinitesimal volume $d\Omega$, $\boldsymbol{\varepsilon}(\boldsymbol{\xi})$ is a local strain at position $\boldsymbol{\xi}$. $\tilde{\Psi}^b$ is the strain smoothing function, $\tilde{\Psi}^b(\boldsymbol{r}) > 0$ for $\|\boldsymbol{r}\| < b$, $\tilde{\Psi}^b(\boldsymbol{r}) = 0$ for $\|\boldsymbol{r}\| \geq b$, and subscript b denotes the radius of influence domain similar to that in Eq. (5). It is assumed that strain smoothing function is continuous in Ω and satisfies the partition of unity property for the reproduction of constant strain field. The strain $\varepsilon(\xi)$

inside the integral of Eq. (9) can be further expressed in terms of $\boldsymbol{\varepsilon}(\mathbf{x})$ and its gradients by the Taylor series expansions:

$$\boldsymbol{\varepsilon}(\xi) = \boldsymbol{\varepsilon}(\mathbf{x}) + \nabla\boldsymbol{\varepsilon}(\mathbf{x}) \cdot (\boldsymbol{\xi} - \mathbf{x}) + \frac{1}{2!} \nabla^{(2)}\boldsymbol{\varepsilon}(\mathbf{x}) \cdot^{(2)} (\boldsymbol{\xi} - \mathbf{x})^{(2)} + O\left(\|\boldsymbol{\xi} - \mathbf{x}\|^3\right) \tag{10}$$

where $\nabla^{(2)}$ denotes the 2nd order gradient operator and $\cdot^{(2)}$ denotes the 2nd order inner product. The symbol $(\varsigma)^{(n)}$ designates the n factor dyadic product $(\varsigma)(\varsigma)\cdots(\varsigma)$ for vector ς. Substituting Eq. (10) into Eq. (9) leads to the following smoothed strain field approximated in terms of unsmoothed (local) strain and its gradients

$$\begin{aligned}
\bar{\boldsymbol{\varepsilon}}^b(\mathbf{x}) &= \int_\Omega \tilde{\Psi}^b(\mathbf{x};\mathbf{x}-\boldsymbol{\xi})\,\boldsymbol{\varepsilon}(\mathbf{x})\,d\Omega \\
&\quad + \int_\Omega \tilde{\Psi}^b(\mathbf{x};\mathbf{x}-\boldsymbol{\xi})\,\nabla\boldsymbol{\varepsilon}(\mathbf{x})\,(\boldsymbol{\xi}-\mathbf{x})\,d\Omega \\
&\quad + \frac{1}{2!}\int_\Omega \tilde{\Psi}^b(\mathbf{x};\mathbf{x}-\boldsymbol{\xi})\,\nabla^{(2)}\boldsymbol{\varepsilon}(\mathbf{x}) \cdot^{(2)} \\
&\quad \times (\boldsymbol{\xi}-\mathbf{x})^{(2)}\,d\Omega + h.o.t \\
&= \boldsymbol{\varepsilon}(\mathbf{x}) \int_\Omega \tilde{\Psi}^b(\mathbf{x};\mathbf{x}-\boldsymbol{\xi})\,d\Omega \\
&\quad + \nabla\boldsymbol{\varepsilon}(\mathbf{x}) \cdot \left(\int_\Omega \tilde{\Psi}^b(\mathbf{x};\mathbf{x}-\boldsymbol{\xi})\,(\boldsymbol{\xi}-\mathbf{x})\,d\Omega\right) \\
&\quad + \nabla^{(2)}\boldsymbol{\varepsilon}(\mathbf{x}) \cdot^{(2)} \left(\frac{1}{2!}\int_\Omega \tilde{\Psi}^b \right. \\
&\quad \left. \times (\mathbf{x};\mathbf{x}-\boldsymbol{\xi})\,(\boldsymbol{\xi}-\mathbf{x})^{(2)}\,d\Omega\right) + h.o.t \\
&= \boldsymbol{\varepsilon}(\mathbf{x}) + \nabla\boldsymbol{\varepsilon}(\mathbf{x}) \cdot \boldsymbol{\lambda}^b(\mathbf{x}) + \nabla^{(2)}\boldsymbol{\varepsilon} \\
&\quad \times (\mathbf{x}) \cdot^{(2)} \boldsymbol{\eta}^b(\mathbf{x}) + h.o.t
\end{aligned} \tag{11}$$

where

$$\boldsymbol{\lambda}^b(\mathbf{x}) = \int_\Omega \tilde{\Psi}^b(\mathbf{x};\mathbf{x}-\boldsymbol{\xi})\,(\boldsymbol{\xi}-\mathbf{x})\,d\Omega \tag{12}$$

$$\boldsymbol{\eta}^b(\mathbf{x}) = \frac{1}{2!}\int_\Omega \tilde{\Psi}^b(\mathbf{x};\mathbf{x}-\boldsymbol{\xi})\,(\boldsymbol{\xi}-\mathbf{x})^{(2)}\,d\Omega \tag{13}$$

$\boldsymbol{\lambda}^b(\mathbf{x})$ and $\boldsymbol{\eta}^b(\mathbf{x})$ define the smoothed position dependent coefficients associated with the first-order and second-order strain gradient, respectively. Similar to the stabilization term in [37], the first-order strain gradient term $\nabla\boldsymbol{\varepsilon}(\mathbf{x}) \cdot \boldsymbol{\lambda}^b(\mathbf{x})$ contains the second-order displacement gradients that can be used for the stabilization of meshfree nodal integration method in this study. Analogously, we have another strain smoothing for regularization

$$\begin{aligned}
\bar{\boldsymbol{\varepsilon}}^c(\mathbf{x}) &= \boldsymbol{\varepsilon}(\mathbf{x}) + \nabla\boldsymbol{\varepsilon}(\mathbf{x}) \cdot \boldsymbol{\lambda}^c(\mathbf{x}) \\
&\quad + \nabla^{(2)}\boldsymbol{\varepsilon}(\mathbf{x}) \cdot^{(2)} \boldsymbol{\eta}^c(\mathbf{x}) + h.o.t
\end{aligned} \tag{14}$$

where

$$\boldsymbol{\lambda}^c(\mathbf{x}) = \int_\Omega \tilde{\Psi}^c(\mathbf{x};\mathbf{x}-\boldsymbol{\xi})\,(\boldsymbol{\xi}-\mathbf{x})\,d\Omega \tag{15}$$

$$\boldsymbol{\eta}^c(\mathbf{x}) = \frac{1}{2!}\int_\Omega \tilde{\Psi}^c(\mathbf{x};\mathbf{x}-\boldsymbol{\xi})\,(\boldsymbol{\xi}-\mathbf{x})^{(2)}\,d\Omega \tag{16}$$

In this study, the second-order strain gradient term $\nabla^{(2)}\boldsymbol{\varepsilon}(\mathbf{x}) \cdot^{(2)} \boldsymbol{\eta}^c(\mathbf{x})$ contains the third-order displacement gradients which will be used for the regularization. With the second-order strain gradient term $\nabla^{(2)}\boldsymbol{\varepsilon}(\mathbf{x}) \cdot^{(2)} \boldsymbol{\eta}^c(\mathbf{x})$, the nonlocal strain field $\bar{\boldsymbol{\varepsilon}}(\mathbf{x})$ in Eq. (7) is now defined by

$$\bar{\boldsymbol{\varepsilon}}(\mathbf{x}) \equiv \boldsymbol{\varepsilon}(\mathbf{x}) + \nabla^{(2)}\boldsymbol{\varepsilon}(\mathbf{x}) \cdot^{(2)} \eta^c(\mathbf{x}) \tag{17}$$

It is worthwhile to mention that $\tilde{\Psi}^b(\mathbf{x})$ in Eq. (11) does not necessary equal to $\tilde{\Psi}^c(\mathbf{x})$ in Eq. (14). In essence, the radius size b of $\tilde{\Psi}^b(\mathbf{x})$ can be considered a numerical length parameter for stabilization while the radius size c of $\tilde{\Psi}^c(\mathbf{x})$ is a material length parameter which can be related to the scale of the microstructure [2] in strain localization problem. Both Eqs. (11) and (14) contain same local strain field $\boldsymbol{\varepsilon}(\mathbf{x})$ but different coefficients in strain gradient terms when sizes $b \neq c$.

In this study we have limited the damage variable to be bonded by $\mathrm{d} < 1$ in Eq. (1) for the weak-discontinuity approach such that the fully damage ($d = 1$) does not occur. This is because the equivalent problem is defined only when $0 \leq \mathrm{d} < 1$. If $d = 1$ is allowed in the damage model, the displacement discontinuities will be initiated due to the loss of ellipticity of the rate equilibrium equations. As a result, a crack will be formed and a strain singularity will thus be unavoidable at the crack tip. The inclusion of fully damage $d = 1$ in the simulation is not within the context of this paper, but will be addressed in the near future for the coupled damage and fracture analysis. In other words, the transition of material degradation from damage ($0 < d < 1$) to fracture ($d = 1$) is not considered in this study and the singular strains/stresses fields near the tip of damage band are not modeled. Under this condition, we can define a damage zone to be

$$\Omega_c = \{\mathbf{x} \in \Omega \mid 0 < d(\mathbf{x}) < 1\} \subset \Omega \tag{18}$$

In the damage zone Ω_c, the discrete non-local strain field is formulated according to the definition of Eq. (17)

$$\bar{\boldsymbol{\varepsilon}}(\mathbf{x}) = \underbrace{\boldsymbol{\varepsilon}(\mathbf{x})}_{local} + \underbrace{\tilde{\bar{\boldsymbol{\varepsilon}}}^c(\mathbf{x})}_{regularization} \quad \forall \mathbf{x} \in \Omega_c \tag{19}$$

where

$$\tilde{\bar{\boldsymbol{\varepsilon}}}^c(\mathbf{x}) = \nabla^{(2)}\boldsymbol{\varepsilon}(\mathbf{x}) \cdot^{(2)} \left(\frac{1}{2!}\int_\Omega \tilde{\Psi}^c(\mathbf{x};\mathbf{x}-\boldsymbol{\xi})\,(\boldsymbol{\xi}-\mathbf{x})^{(2)}\,d\Omega\right) \tag{20}$$

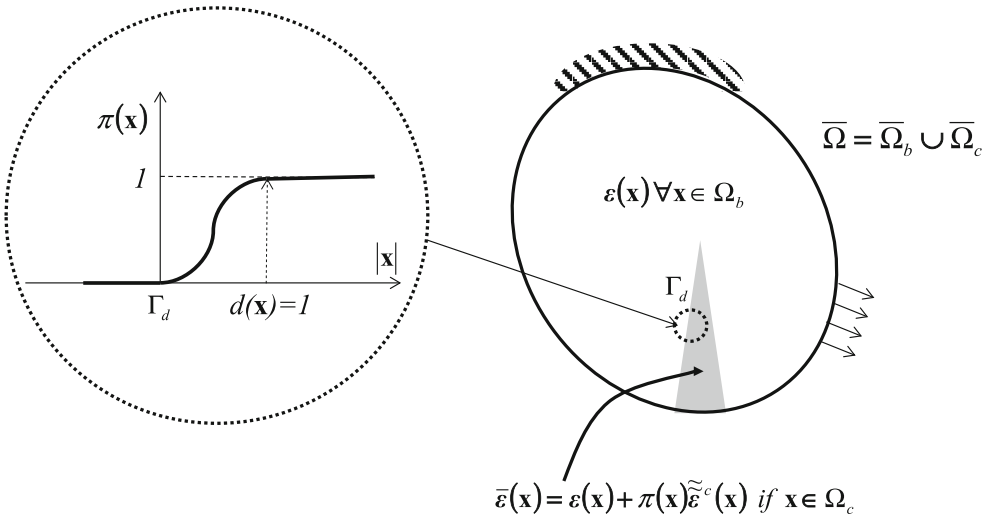

Fig. 1 The meshfree morphing model for local and non-local strain approximations

The term $\tilde{\tilde{\boldsymbol{\varepsilon}}}^c$ contains the third-order derivatives of displacements and is introduced to the regularization of the meshfree nodal integration solution in damage-induced strain localization problem. The second-order strain gradient $\tilde{\tilde{\boldsymbol{\varepsilon}}}^c$ brings in the non-locality into the analysis of strain localization problem, which resembles the standard second-order derivative of strains in the gradient-type damage model [1]. Analogously, we can also define the undamaged zone to be $\Omega_b = \{\mathbf{x} \in \Omega \ | d(\mathbf{x}) = 0\}$ such that $\bar{\Omega} = \bar{\Omega}_b \cup \bar{\Omega}_c$ and $\boldsymbol{\Gamma}_d = \bar{\Omega}_b \cap \bar{\Omega}_c$. Note $\boldsymbol{\Gamma}_d$ is a moving interface which travels with the evolution of monotone non-decreasing damage d.

Ideally, one would like to couple the nonlocal strain $\bar{\boldsymbol{\varepsilon}}(\mathbf{x})$ with local strain $\boldsymbol{\varepsilon}(\mathbf{x})$ as a continuum model for the meshfree regularization of solution in strain localization problems. Obviously a direct coupling method introduces the non-uniqueness of strain along their bounding interface $\boldsymbol{\Gamma}_d$ as

$$[[\bar{\boldsymbol{\varepsilon}}]]_{\boldsymbol{\Gamma}_d} = \bar{\boldsymbol{\varepsilon}}(\mathbf{x}) - \boldsymbol{\varepsilon}(\mathbf{x}) = \tilde{\tilde{\boldsymbol{\varepsilon}}}^c(\mathbf{x}) \neq 0 \quad for\ \mathbf{x} \in \boldsymbol{\Gamma}_d \tag{21}$$

In other words, an introduction of a direct coupling method to the Galerkin meshfree method leads to an undefined strain field near the damage zone.

To resolve this problem, a continuum coupling model is presented in this study by incorporating a morphing function $\boldsymbol{\pi}(\mathbf{x})$ in Eq. (19), such that

$$\bar{\boldsymbol{\varepsilon}}(\mathbf{x}) \equiv \underbrace{\boldsymbol{\varepsilon}(\mathbf{x})}_{local} + \underbrace{\boldsymbol{\pi}(\mathbf{x})\tilde{\tilde{\boldsymbol{\varepsilon}}}^c(\mathbf{x})}_{regularization} \ \forall \mathbf{x} \in \Omega_c \tag{22}$$

and

$$\bar{\boldsymbol{\varepsilon}}(\mathbf{x}) = \boldsymbol{\varepsilon}(\mathbf{x}) \quad for\ \mathbf{x} \in \boldsymbol{\Gamma}_d \tag{23}$$

Clearly, the morphing function $\boldsymbol{\pi}(\mathbf{x})$ has to be continuous in damage zone Ω_c and satisfies $\boldsymbol{\pi}(\mathbf{x}) = 0 \ \forall \mathbf{x} \in \boldsymbol{\Gamma}_d$ and $0 \leq \boldsymbol{\pi}(\mathbf{x}) \leq 1 \ \forall \mathbf{x} \in \Omega_c$. Combination of Eqs. (22) and (23) gives

$$\boldsymbol{\pi}(\mathbf{x})\tilde{\tilde{\boldsymbol{\varepsilon}}}^c(\mathbf{x}) = 0 \ \forall \mathbf{x} \in \boldsymbol{\Gamma}_d \tag{24}$$

There are many possible choices for the determination of morphing function. One of the simple choices is to make the morphing function $\boldsymbol{\pi}(\mathbf{x})$ to be a linear or higher-order function of damage variable $d(\mathbf{x})$. In this study, the morphing function is chosen to be

$$\boldsymbol{\pi}(\mathbf{x}) = d(\mathbf{x}) \ \forall \mathbf{x} \in \Omega_c \tag{25}$$

With the above morphing function, the result of Eq. (24) yields the following homogenous jump condition in the coupled strain field

$$[[\bar{\boldsymbol{\varepsilon}}]]_{\boldsymbol{\Gamma}_d} = \bar{\boldsymbol{\varepsilon}}(\mathbf{x}) - \boldsymbol{\varepsilon}(\mathbf{x}) = 0 \quad for\ \mathbf{x} \in \boldsymbol{\Gamma}_d \tag{26}$$

As a result, the coupled strain field is uniquely determined in the whole meshfree computation domain. The coupling of local and nonlocal strain models is illustrated in Fig. 1.

4 Variational formulation and discrete equations

To introduce the stabilization and regularization strain fields into the Galerkin method, we follow closely the work in [37]. A review of strain gradient stabilization (SGS) method [37] for linear elasticity is given in Appendix. The discrete weak form for linear elasticity can be extended to cover the nonlinear cases through an updated Lagrangian formulation with reference to the current configuration in the elastic-damage analysis:

$$\delta\overline{\Pi} = \int_{\Omega} \delta\left(\boldsymbol{\varepsilon}\left(\hat{\boldsymbol{u}}\right)\right)^{T} : \boldsymbol{\sigma}\, d\Omega + \int_{\Omega} \delta\left(\nabla\boldsymbol{\varepsilon}\left(\hat{\boldsymbol{u}}\right)\cdot\boldsymbol{\lambda}^{b}\right)^{T} : \tilde{\boldsymbol{\sigma}}\, d\Omega - l^{ext}\left(\hat{\boldsymbol{u}}\right) \tag{27}$$

where $\boldsymbol{\sigma}$ is the local Cauchy stress obtained by direct nodal integration scheme and $\tilde{\boldsymbol{\sigma}}$ is the enhanced stress field for stabilization. Note that both stress quantities are defined at the current configuration Ω. l^{ext} corresponds to the nonlinear version of external work. The enhanced stress field for stabilization in the nonlinear analysis is obtained by replacing the elastic tensor $\boldsymbol{C}$ using a material response tensor (elasto-damage tangent modulus) $\boldsymbol{C}^{\sigma}$ [6] as

$$\tilde{\boldsymbol{\sigma}} = \boldsymbol{C}^{\sigma} : \left(\nabla\boldsymbol{\varepsilon}\left(\hat{\boldsymbol{u}}\right)\cdot\boldsymbol{\lambda}^{b}\right) \tag{28}$$

Equation (28) indicates that the enhanced stresses are related to the first-order special derivatives of strains through the elasto-damage tangent modulus. The linearization of Eq. (27) with a neglect of non-linear contribution from the nodal strain and enhanced strain fields in the elastic-damage material yields

$$\Delta\delta\overline{\Pi} = \int_{\Omega} \delta\left(\boldsymbol{\varepsilon}\left(\hat{\boldsymbol{u}}\right)\right)^{T} : \left(\boldsymbol{C}^{\sigma}\right) : \Delta\left(\boldsymbol{\varepsilon}\left(\hat{\boldsymbol{u}}\right)\right) d\Omega + \int_{\Omega} \delta\left(\nabla\boldsymbol{\varepsilon}\left(\hat{\boldsymbol{u}}\right)\cdot\boldsymbol{\lambda}^{b}\right)^{T} : \boldsymbol{C}^{\sigma} : \Delta \times \left(\nabla\boldsymbol{\varepsilon}\left(\hat{\boldsymbol{u}}\right)\cdot\boldsymbol{\lambda}^{b}\right) d\Omega - \Delta l^{ext} \tag{29}$$

Considering that the Lagrangian meshfree shape function [7] and the gradients of displacement and strain approximations are defined in the un-deformed configuration to avoid any tensile instability, the variation equation of Eq. (29) is transformed from the current configuration Ω to the un-deformed configuration Ω^0 as

$$\Delta\delta\overline{\Pi} = \int_{\Omega^0} \delta\left(\boldsymbol{F}^{-1}\boldsymbol{\varepsilon}\right)^{T} : \left(\boldsymbol{C}^{\sigma}\right) : \Delta\left(\boldsymbol{F}^{-1}\boldsymbol{\varepsilon}\right) J^{0} d\Omega + \int_{\Omega^0} \delta\left(\boldsymbol{F}^{-1}\left(\nabla\boldsymbol{\varepsilon}\cdot\boldsymbol{\lambda}^{b}\right)\right)^{T} : \boldsymbol{C}^{\sigma} : \Delta \times \left(\boldsymbol{F}^{-1}\left(\nabla\boldsymbol{\varepsilon}\cdot\boldsymbol{\lambda}^{b}\right)\right) J^{0} d\Omega - \Delta l^{ext} \tag{30}$$

$$F_{ij}\left(\mathbf{X}\right) = \frac{\partial x_i\left(\mathbf{X}\right)}{\partial X_j} = \sum_{I=1}^{NP} \frac{\partial \phi^{a}\left(\mathbf{X}\right)}{\partial X_j} x_{Ii} \tag{31}$$

where $\boldsymbol{F}$ is the deformation gradient, x_{Ii} denotes the i-component of current position at node I, and $\boldsymbol{X} = [\mathrm{X}, \mathrm{Y}]^{\mathrm{T}}$ is a position vector defined in the un-deformed configuration. J^0 is the determinant of the deformation gradient.

Using the first-order meshfree convex approximation [33] for $\phi^{a}\left(\mathbf{X}\right)$ and zero-order strain smoothing function for $\tilde{\Psi}^{b}\left(\mathbf{X}\right)$ and $\tilde{\Psi}^{c}\left(\mathbf{X}\right)$ leads to the following regularized incremental discrete equations to be solved in the damage-induced strain localization analysis:

$$\left(\boldsymbol{K}^{\boldsymbol{M}} + \tilde{\boldsymbol{K}}\right)_{n+1}^{v} \left(\Delta\tilde{\boldsymbol{U}}\right)_{n+1}^{v+1} = \mathbf{R}_{n+1}^{v} \tag{32}$$

where all the functions are computed in the v-th iteration during the $(n+1)$-th time incremental step. The material stiffness matrices $\boldsymbol{K}^{\boldsymbol{M}}$ using the direct nodal integration (DNI) scheme is given by

$$\boldsymbol{K}_{IJ}^{M} = \int_{\Omega^0} \boldsymbol{B}_I^{T} \boldsymbol{C}^{\sigma} \boldsymbol{B}_J J^{0} d\Omega \overset{DNI}{=} \sum_{K=1}^{NP} \boldsymbol{B}_I^{T}\left(\mathbf{X}_K\right) \boldsymbol{C}^{\sigma} \boldsymbol{B}_J\left(\mathbf{X}_K\right) J^{0}\left(\mathbf{X}_K\right) V_K^{0} \tag{33}$$

where

$$\boldsymbol{B}_I\left(\mathbf{X}\right) = \begin{bmatrix} b_{I1}\left(\mathbf{X}\right) & 0 \\ b_{I2}\left(\mathbf{X}\right) & b_{I1}\left(\mathbf{X}\right) \\ 0 & b_{I2}\left(\mathbf{X}\right) \end{bmatrix} \tag{34}$$

$$b_{I1}\left(\mathbf{X}\right) = \phi_{I,x}^{a}\left(\mathbf{X}\right) \text{ and } b_{I2}\left(\mathbf{X}\right) = \phi_{I,y}^{a}\left(\mathbf{X}\right) \tag{35}$$

The stabilized stiffness counterpart $\tilde{\boldsymbol{K}}_{IJ}$ using the direct nodal integration scheme can be expressed by

$$\tilde{\boldsymbol{K}}_{IJ} = \int_{\Omega^0} \tilde{\boldsymbol{B}}_I^{T} \boldsymbol{C}^{\sigma} \tilde{\boldsymbol{B}}_J J^{0} d\Omega \overset{DNI}{=} \sum_{K=1}^{NP} \tilde{\boldsymbol{B}}_I^{T}\left(\mathbf{X}_K\right) \boldsymbol{C}^{\sigma} \tilde{\boldsymbol{B}}_J\left(\mathbf{X}_K\right) J^{0}\left(\mathbf{X}_K\right) V_K^{0} \tag{36}$$

where the first-order strain-gradient matrix $\tilde{B}_I$ is given by

$$\tilde{\boldsymbol{B}}_I\left(\mathbf{X}\right) = \begin{bmatrix} \tilde{b}_{I1}\left(\mathbf{X}\right) & 0 \\ \tilde{b}_{I2}\left(\mathbf{X}\right) & \tilde{b}_{I1}\left(\mathbf{X}\right) \\ 0 & \tilde{b}_{I2}\left(\mathbf{X}\right) \end{bmatrix} \tag{37}$$

The components of the first-order strain-gradient matrix $\tilde{\boldsymbol{B}}_I$ are

$$\tilde{b}_{I1}\left(\mathbf{X}\right) = \beta_x\left(\mathbf{X}\right)\phi_{I,xx}^{a}\left(\mathbf{X}\right) + \beta_y\left(\mathbf{X}\right)\phi_{I,xy}^{a}\left(\mathbf{X}\right) \tag{38}$$

$$\tilde{b}_{I2}\left(\mathbf{X}\right) = \beta_x\left(\mathbf{X}\right)\phi_{I,yx}^{a}\left(\mathbf{X}\right) + \beta_y\left(\mathbf{X}\right)\phi_{I,yy}^{a}\left(\mathbf{X}\right) \tag{39}$$

$$\beta_x\left(\mathbf{X}\right) = \sum_{J=1}^{NP} \tilde{\Psi}_J^{b}\left(\mathbf{X}\right)\left(X_J - X\right) \tag{40}$$

$$\beta_y\left(\mathbf{X}\right) = \sum_{J=1}^{NP} \tilde{\Psi}_I^{b}\left(\mathbf{X}\right)\left(Y_J - Y\right) \tag{41}$$

Correspondingly, the residual term along with the stabilized internal force term are expressed in a conventional way by

$$\mathbf{R} = \boldsymbol{f}^{ext} - \boldsymbol{f}^{int} - \tilde{\boldsymbol{f}}^{stab} \tag{42}$$

where $\boldsymbol{f}^{ext}$ is standard external force vector. The internal force vector is computed by the direct nodal integration scheme as

$$\boldsymbol{f}_I^{int} = \int_{\Omega^0} \boldsymbol{B}_I^T \boldsymbol{\sigma} \boldsymbol{J}^0 d\Omega \overset{DNI}{=} \sum_{K=1}^{NP} \boldsymbol{B}_I^T \left(\mathbf{X}_K\right) \boldsymbol{\sigma} \left(\mathbf{X}_K\right) J^0 V_K^0 \tag{43}$$

where $\boldsymbol{\sigma}^T = (\sigma_{11}, \sigma_{12}, \sigma_{22})$ is the Cauchy stress for internal force calculation. The stabilized force vector $\tilde{\boldsymbol{f}}^{stab}$ will be given later in the same section.

Without the incorporation of regularization strain field, Eq. (30) represents a case of local model where the stress at a given point is assumed to be uniquely determined by the strain history at this point. As damage-induced strain field localizes over narrow zones of a continuum, statistical homogeneity in a representative material volume is lost. This local form of quasi-static meshfree formulation in Eq. (30) will exhibit the pathological localization of deformation and requires regularization. For that reason, a nonlocal strain defined in Eq. (22) is used for the computation of nonlocal equivalent strain to regularize the localized solution.

Using the stress–strain relationship in Eq. (1) for the scalar isotropic elastic-damage model, the change of the Cauchy stress at $(v+1)$-th iteration is

$$\begin{aligned}\Delta\boldsymbol{\sigma}_{n+1}^{v+1} = &\left(1 - d_{n+1}^v \left(\bar{\varepsilon}_{eq,n+1}^v\right)\right) \boldsymbol{C} : \Delta\boldsymbol{\varepsilon}_{n+1}^{v+1} \\ &- \left(\boldsymbol{C} : \boldsymbol{\varepsilon}_{n+1}^v\right) \Delta d_{n+1}^{v+1} \left(\bar{\varepsilon}_{eq,n+1}^{v+1}\right)\end{aligned} \tag{44}$$

where the change of damage variable Δd_{n+1}^{v+1} based on the nonlocal equivalent strain in Eq. (8) is computed by

$$\Delta d_{n+1}^{v+1} = \left(g_\kappa\right)_{n+1}^v \Delta \left(\bar{\varepsilon}_{eq}\right)_{n+1}^{v+1} \tag{45}$$

with

$$\left(g_k\right)_{n+1}^v = \begin{cases} 0 & \text{if } \left(\bar{\varepsilon}_{eq}\right)_{n+1}^v < \kappa_n^0 \\ \left(\frac{dg}{d\kappa}\right)_{n+1}^v & \text{otherwise} \end{cases} \tag{46}$$

and the incremental nonlocal equivalent strain is computed by

$$\begin{aligned}\Delta \left(\bar{\varepsilon}_{eq}\right)_{n+1}^{v+1} &= \frac{1}{E \left(\bar{\varepsilon}_{eq}\right)_{n+1}^v} \left(\boldsymbol{C} : \bar{\boldsymbol{\varepsilon}}_{\boldsymbol{n+1}}^v\right) : \Delta\bar{\boldsymbol{\varepsilon}}_{n+1}^{v+1} \\ &= \boldsymbol{\Xi}_{n+1}^v : \Delta\bar{\boldsymbol{\varepsilon}}_{n+1}^{v+1}\end{aligned} \tag{47}$$

where

$$\boldsymbol{\Xi}_{n+1}^v = \frac{1}{E \left(\bar{\varepsilon}_{eq}\right)_{n+1}^v} \left(\boldsymbol{C} : \bar{\varepsilon}_{n+1}^v\right) \tag{48}$$

κ_n^0 in Eq. (46) denotes the converged value of equivalent strain at n-th incremental step. The nonlocal strain increment $\Delta\bar{\boldsymbol{\varepsilon}}_{n+1}^{v+1}$ in Eq. (47) can be obtained according to the definition of morphed strain in Eq. (22) and computed by

$$\begin{aligned}\Delta\bar{\boldsymbol{\varepsilon}}_{n+1}^{v+1} &= \left(\boldsymbol{B}\right)_{n+1}^v \Delta\tilde{\boldsymbol{U}}_{n+1}^{v+1} + d_{n+1}^v \left(\tilde{\tilde{\boldsymbol{B}}}\right)_{n+1}^v \Delta\tilde{\boldsymbol{U}}_{n+1}^{v+1} \\ &\quad + \Delta d_{n+1}^{v+1} \left(\tilde{\tilde{\boldsymbol{B}}}\right)_{n+1}^v \tilde{\boldsymbol{U}}_{n+1}^v \\ &= \left[\left(\boldsymbol{B}\right)_{n+1}^v + d_{n+1}^v \left(\tilde{\tilde{\boldsymbol{B}}}\right)_{n+1}^v\right] \Delta\tilde{\boldsymbol{U}}_{n+1}^{v+1} \\ &\quad + \Delta d_{n+1}^{v+1} \left(\tilde{\tilde{\boldsymbol{B}}}\right)_{n+1}^v \tilde{\boldsymbol{U}}_{n+1}^v\end{aligned} \tag{49}$$

where

$$\tilde{\tilde{\boldsymbol{B}}}_I \left(\mathbf{X}\right) = \begin{bmatrix} \tilde{\tilde{b}}_{I1} \left(\mathbf{X}\right) & 0 \\ \tilde{\tilde{b}}_{I2} \left(\mathbf{X}\right) & \tilde{\tilde{b}}_{I1} \left(\mathbf{X}\right) \\ 0 & \tilde{\tilde{b}}_{I2} \left(\mathbf{X}\right) \end{bmatrix} \tag{50}$$

Their components are

$$\begin{aligned}\tilde{\tilde{b}}_{I1} \left(\mathbf{X}\right) = &\alpha_{xx} \left(\mathbf{X}\right) \phi_{I,xxx}^a \left(\mathbf{X}\right) + 2\alpha_{xy} \phi_{I,xxy}^a \left(\mathbf{X}\right) \\ &+ \alpha_{yy} \left(\mathbf{X}\right) \phi_{I,xyy}^a \left(\mathbf{X}\right)\end{aligned} \tag{51}$$

$$\begin{aligned}\tilde{\tilde{b}}_{I2} \left(\mathbf{X}\right) = &\alpha_{xx} \left(\mathbf{X}\right) \phi_{I,yxx}^a \left(\mathbf{X}\right) \\ &+ 2\alpha_{xy} \phi_{I,yxy}^a \left(\mathbf{X}\right) + \alpha_{yy} \left(\mathbf{X}\right) \phi_{I,yyy}^a \left(\mathbf{X}\right)\end{aligned} \tag{52}$$

$$\alpha_{xx} \left(\mathbf{X}\right) = \frac{1}{2} \sum_{J=1}^{NP} \tilde{\Psi}_J^c \left(\mathbf{X}\right) \left(X_J - X\right)^2 \tag{53}$$

$$\alpha_{xy} \left(\mathbf{X}\right) = \frac{1}{2} \sum_{J=1}^{NP} \tilde{\Psi}_J^c \left(\mathbf{X}\right) \left(X_J - X\right) \left(Y_J - Y\right) \tag{54}$$

$$\alpha_{yy} \left(\mathbf{X}\right) = \frac{1}{2} \sum_{J=1}^{NP} \tilde{\Psi}_J^c \left(\mathbf{X}\right) \left(Y_J - Y\right)^2 \tag{55}$$

Substituting Eq. (49) into Eq. (47) yields the incremental nonlocal equivalent strain to be computed by

$$\begin{aligned}\Delta \left(\bar{\varepsilon}_{eq}\right)_{n+1}^{v+1} = &\frac{1}{E \left(\bar{\varepsilon}_{eq}\right)_{n+1}^v} \\ &\times \left(\boldsymbol{C} : \bar{\boldsymbol{\varepsilon}}_{n+1}^v\right) : \left\{\left[\left(\boldsymbol{B}\right)_{n+1}^v + d_{n+1}^v \left(\tilde{\tilde{\boldsymbol{B}}}\right)_{n+1}^v\right]\right. \\ &\left.\times \Delta\tilde{\boldsymbol{U}}_{n+1}^{v+1} + \Delta d_{n+1}^{v+1} \left(\tilde{\tilde{\boldsymbol{B}}}\right)_{n+1}^v \tilde{\boldsymbol{U}}_{n+1}^v\right\}\end{aligned} \tag{56}$$

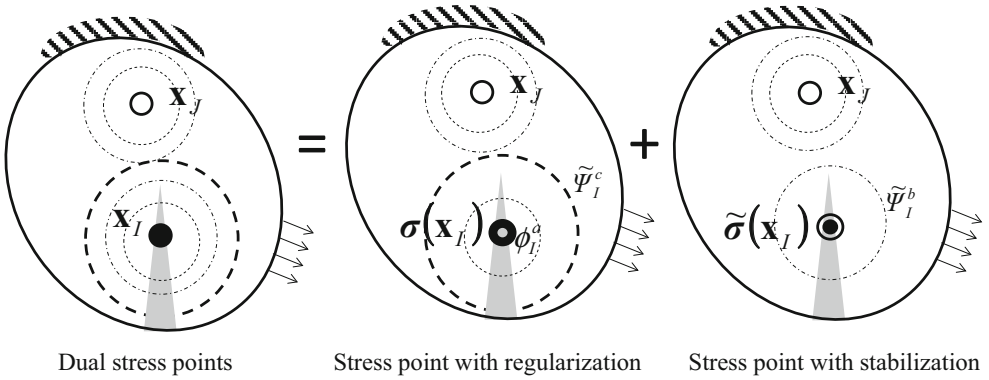

Fig. 2 Illustration of dual stress points in present meshfree nodal integration scheme for the elastic-damage induced strain localization problem

Subsequently, the substitution of Eqs. (46)–(49) into Eq. (45) yields

$$\Delta d_{n+1}^{v+1} = \frac{(g_k)_{n+1}^{v}\, \boldsymbol{\Xi}_{n+1}^{v} : \left[(\boldsymbol{B})_{n+1}^{v} + d_{n+1}^{v} \left(\tilde{\tilde{\boldsymbol{B}}} \right)_{n+1}^{v} \right] \Delta \tilde{\boldsymbol{U}}_{n+1}^{v+1}}{1 - (g_k)_{n+1}^{v}\, \boldsymbol{\Xi}_{n+1}^{v} : \left(\tilde{\tilde{\boldsymbol{B}}} \right)_{n+1}^{v} \tilde{\boldsymbol{U}}_{n+1}^{v}} \tag{57}$$

which is used to update the damage variable. Subsequently, the elasto-damage tangent modulus $\boldsymbol{C}^{\sigma}$ is obtained using the algorithmic relationship in Eq. (44) to yield

$$\left. \frac{d\boldsymbol{\sigma}}{d\boldsymbol{\varepsilon}} \right|_{n+1} = \boldsymbol{C}_{n+1}^{\sigma} = (1 - d_{n+1})\, \boldsymbol{C} - (g_k)_{n+1} \times \frac{\left[\boldsymbol{C} : \boldsymbol{\varepsilon}_{n+1} \right] \otimes \left[(\boldsymbol{C} : \bar{\boldsymbol{\varepsilon}}_{n+1}) : \partial_{\boldsymbol{\varepsilon}} \bar{\boldsymbol{\varepsilon}}_{n+1} \right]}{E \left(\bar{\boldsymbol{\varepsilon}}_{eq} \right)_{n+1}} \tag{58}$$

The term $\partial_{\boldsymbol{\varepsilon}} \bar{\varepsilon}_{n+1}$ in Eq. (66) can be further approximated by

$$\partial_{\boldsymbol{\varepsilon}} \bar{\boldsymbol{\varepsilon}}_{n+1} = \boldsymbol{I} + (g_k)_{n+1}\, \tilde{\tilde{\boldsymbol{\varepsilon}}}_{n+1}^{c} + h.o.t \approx \boldsymbol{I} + (g_k)_{n+1}\, \tilde{\tilde{\boldsymbol{\varepsilon}}}_{n+1}^{c} \tag{59}$$

The term $(1 - d_{n+1})\ \boldsymbol{C}$ in Eq. (58) represents the secant tangent modulus. The second term on the RHS of Eq. (58) is a corrective tangent modulus due to the damage growth, and this term is always non-symmetric.

Finally, the stabilized force vector is also computed by the direct nodal integration scheme as

$$\tilde{\boldsymbol{f}}_I^{stab} = \int_{\Omega^0} \tilde{\boldsymbol{B}}_I^T \tilde{\boldsymbol{\sigma}}\, J^0 d\Omega \overset{DNI}{=} \sum_{K=1}^{NP} \tilde{\boldsymbol{B}}_I^T \left(\mathbf{X}_K \right) \tilde{\boldsymbol{\sigma}} \left(\mathbf{X}_K \right) J^0 V_K^0 \tag{60}$$

where $\tilde{\boldsymbol{\sigma}}^T = (\tilde{\sigma}_{11}, \tilde{\sigma}_{12}, \tilde{\sigma}_{22})$ is a vector containing the component of Cauchy stress associated with the stabilization and is updated by

$$\tilde{\boldsymbol{\sigma}}_{n+1}^{v+1} = \tilde{\boldsymbol{\sigma}}_{n}^{v} + \Delta \tilde{\boldsymbol{\sigma}}_{n+1}^{v+1} = \tilde{\boldsymbol{\sigma}}_{n}^{v} + \left(\boldsymbol{C}^{\sigma} \right)_{n+1}^{v} \left(\tilde{\tilde{\boldsymbol{B}}} \right)_{n+1}^{v} \Delta \tilde{\boldsymbol{U}}_{n+1}^{v+1} \tag{61}$$

The computation of Eq. (32) involves two stress points at each meshfree node, one for nodal stress $\boldsymbol{\sigma}$ with regularization effect as needed and the other for the enhanced nodal stress $\tilde{\boldsymbol{\sigma}}$ for the necessary stabilization. This dual stress point integration scheme is illustrated in Fig 2.

5 Numerical examples

In this section, three benchmark examples are analyzed to study the performance of present method in the elastic-damage induced strain localization problems. Plain stress condition is assumed in two-dimensional problems. Unless otherwise specified, a normalized nodal support size of 1.3 is used for the radius size of meshfree shape functions $\phi^a(\mathbf{x})$ and strain smoothing function $\tilde{\Psi}^b(\mathbf{x})$ for stabilization. In all test cases, we have used the first-order meshfree convex approximations [33] for meshfree shape functions $\phi^a(\mathbf{x})$ in displacement approximation to simplify the boundary condition enforcement. The Shepard function [33] is considered to for the strain smoothing function $\tilde{\Psi}^b(\mathbf{x})$ and $\tilde{\Psi}^c(\mathbf{x})$ in this study. A standard Newton-Raphson method and automatic time steps are employed to solve the nonlinear equation (32).

The damage law defined in Eq. (2) is taken to be [8]

$$g(\kappa) = \begin{cases} \dfrac{\kappa_c (\kappa - \kappa_i)}{\kappa (\kappa_c - \kappa_i)} & \text{if } \kappa_i \le \kappa \le \kappa_c \\ 0.99 & \text{if } \kappa > \kappa_c \end{cases} \tag{62}$$

where κ_i and κ_c denotes the initial and critical values of internal variable κ, respectively. When damage variable reaches 0.99, the program will stop the run.

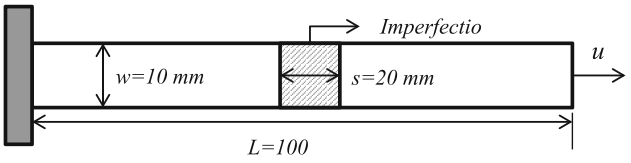

Fig. 3 The 2D bar model

5.1 2D bar in simple tension test

The first example studies a 2D bar in tension. The geometry and boundary conditions of the bar are shown in Fig. 3. The bar has Young's modulus $E = 2.0 \times 10^6$ N/mm^2, and Poisson's ratio v is assumed to be zero to mimic the uniaxial deformation as in one-dimensional problem. The following damage parameters are used: $\kappa_i = 1.0 \times 10^{-4}$, and $\kappa_c = 5.0 \times 10^{-3}$. In order to initiate strain localization, an initial imperfection is placed in the central area of the bar with a reduction of 5 % in the Young's modulus.

Four levels of refinements in the discretization, namely 20×1, 40×1, 60×1, 80×1 elements are used to study the sensitivity of the discretization in the present method. A radius size c of $\tilde{\Psi}^c(\mathbf{x})$ in Eq. (18) is taken to be 20 mm for the calculation of regularized strain in all spatial discretization. The force–displacement curves in Fig 4a demonstrate the discretization-insensitive results using the proposed method. Figure 4b presents the comparison of regularized strain profiles which agree very well with each other. Corresponding, the damage profiles are shown in Fig. 4c which is an analogue of the regularized strain profiles. Apparently in this degenerated 1D bar problem, the damage distribution produced by the present method is not sensitive to the discretization.

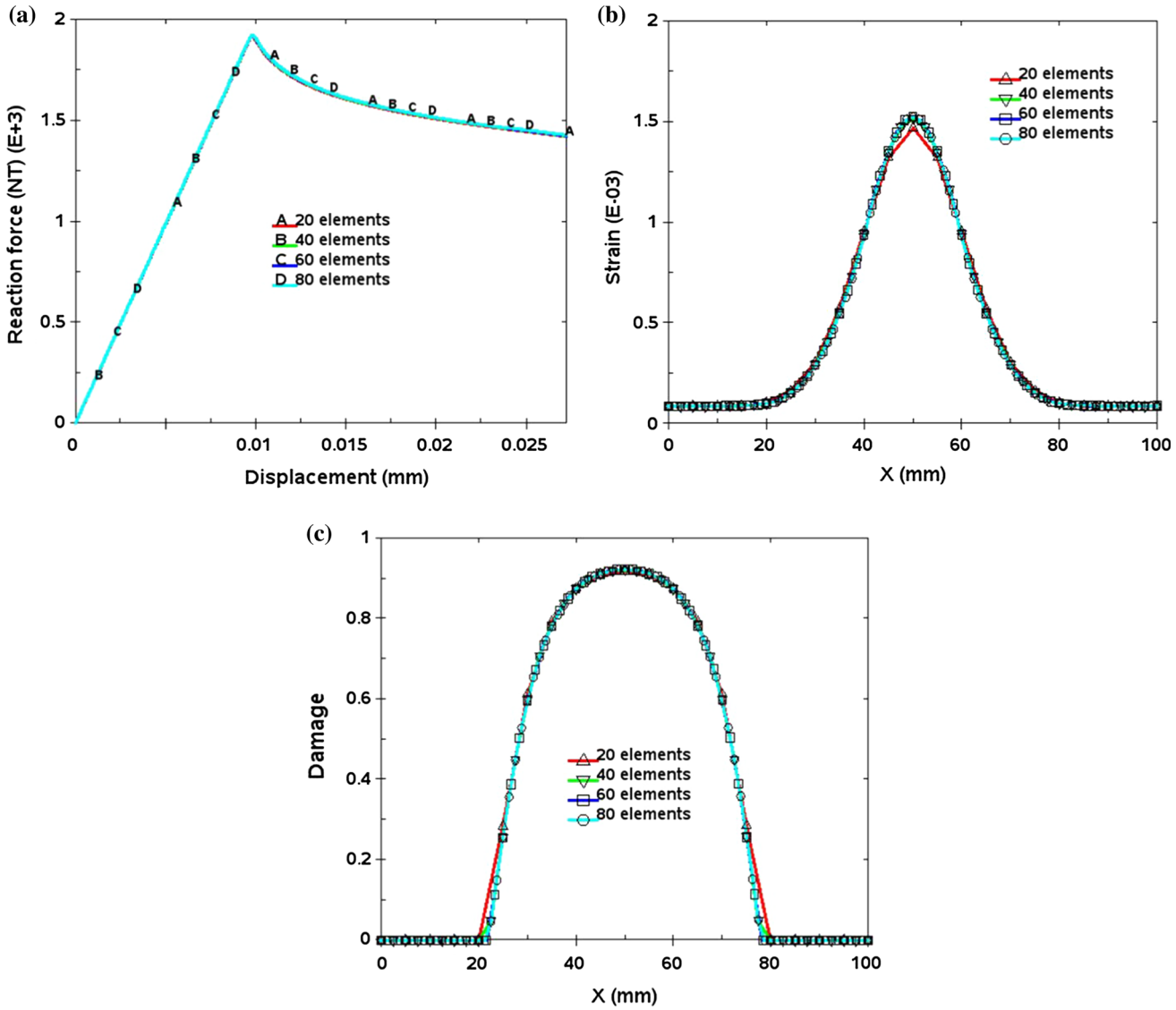

Fig. 4 The convergence study of 2D bar model. **a** Force–displacement curves, **b** strain profiles, **c** damage profiles

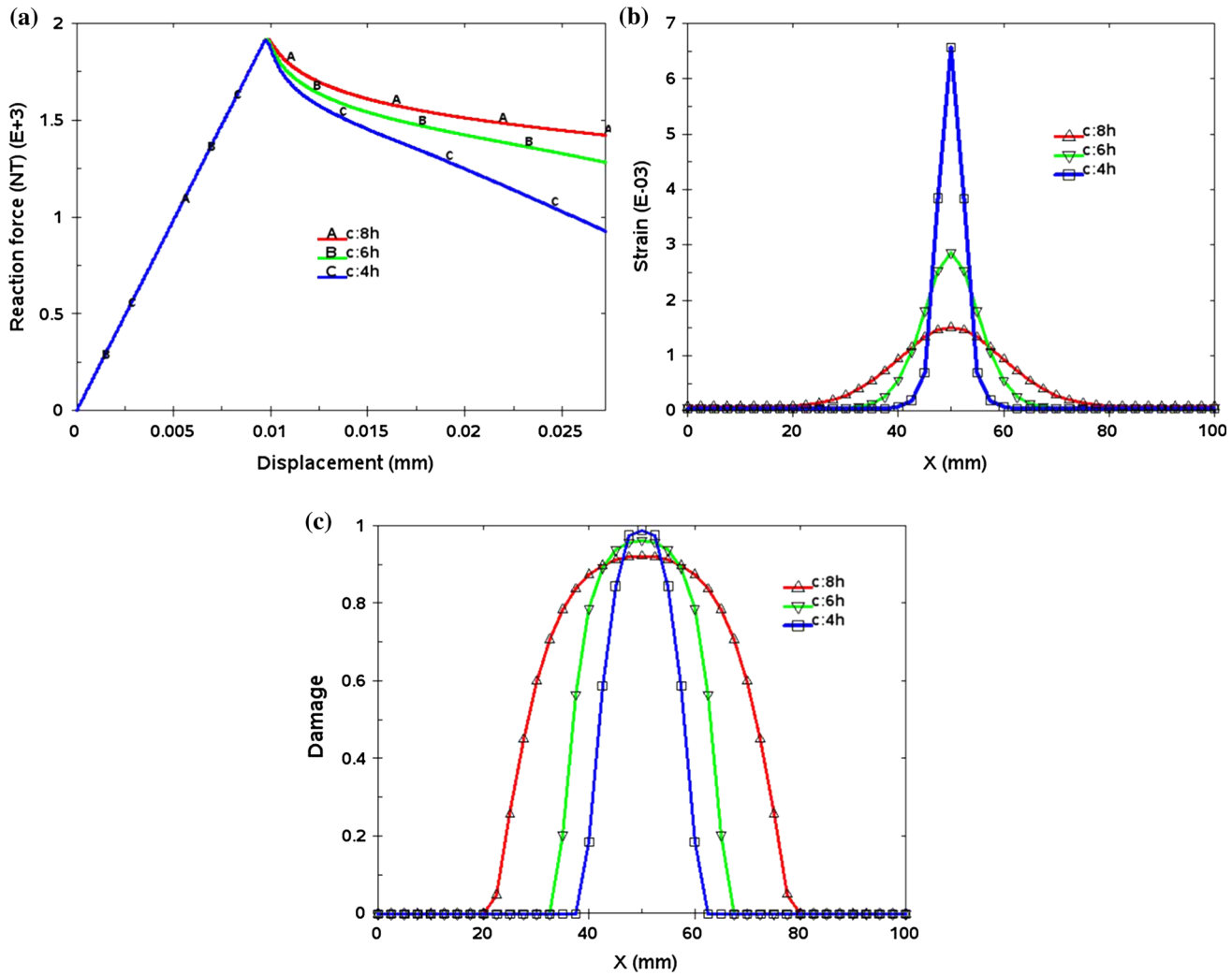

Fig. 5 The regularization effect of 2D bar model with a discretization of 40 × 1 elements. **a** Force–displacement curves, **b** strain profiles, **c** damage profiles

The regularization effect of radius size c is also studied using the discretization with 40 × 1 elements. Three radii of c, 10 mm (4 h), 15 mm (6 h) and 20 mm (8 h), are considered where h denotes the element size in the discretization. Figure 5a presents the comparison of force–displacement curves due to different regularization effects. Obviously the larger size of radius used in the strain regularization, the larger bandwidth of strain and damage profiles are as shown in Fig. 5b, c, respectively.

5.2 Single edge-notch problem

This example deals with a single edge-notch in two-dimensional problem. The problem statement including the boundary condition and geometrical information is shown in Fig. 6. The material constants are set to: Young's mod-

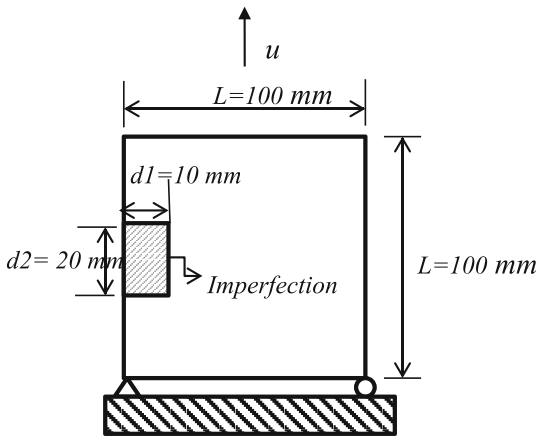

Fig. 6 The single edge-notch model

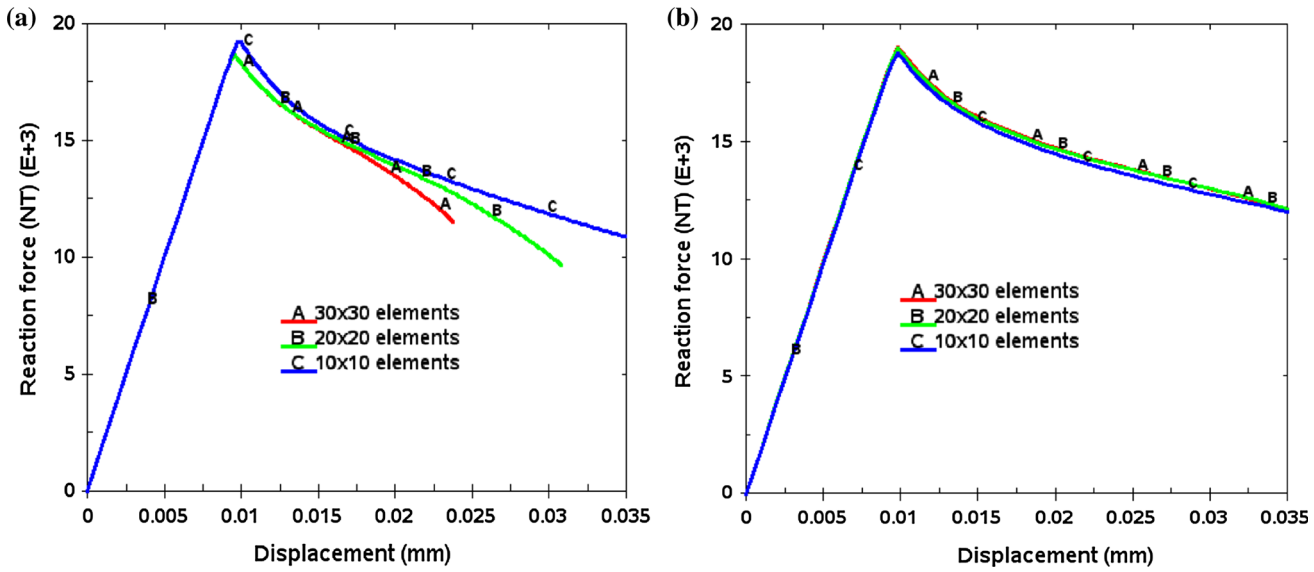

Fig. 7 The convergence of force–displacement curves. **a** FEM. **b** Present method

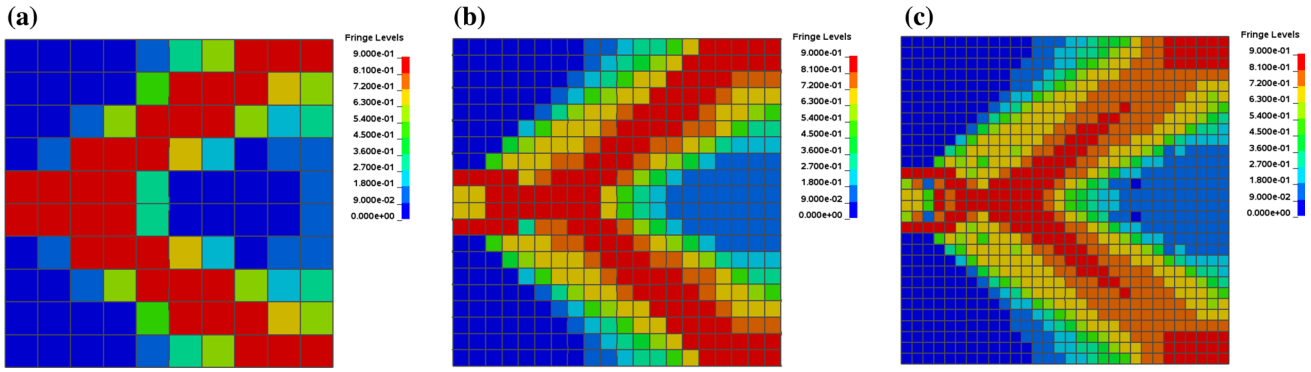

Fig. 8 Comparison of damage contour in FEM. **a** 10 × 10 elements, **b** 20 × 20 elements, **c** 30 × 30 elements

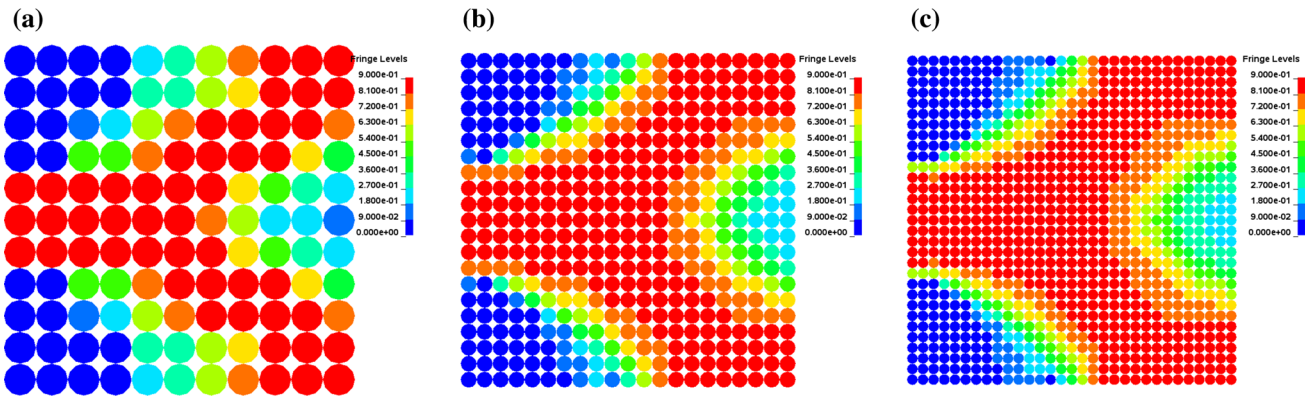

Fig. 9 Comparison of damage contour in present method. **a** 10 × 10 elements, **b** 20 × 20 elements, **c** 30 × 30 elements

ulus $E = 2.0 \times 10^6$ N/mm^2, Poisson's ratio $v = 0.2$, $\kappa_i = 1.0 \times 10^{-4}$, and $\kappa_c = 5.0 \times 10^{-3}$. The initial imperfection has a 30 % reduction of strength in the Young's modulus. The radius size c of $\tilde{\Psi}^c(\mathbf{x})$ for regularization is taken to be 10 mm. The result of finite element method using bi-linear element is considered for comparison.

The convergence of reaction force response in finite element solution is given in Fig. 7a. As expected, the patho-

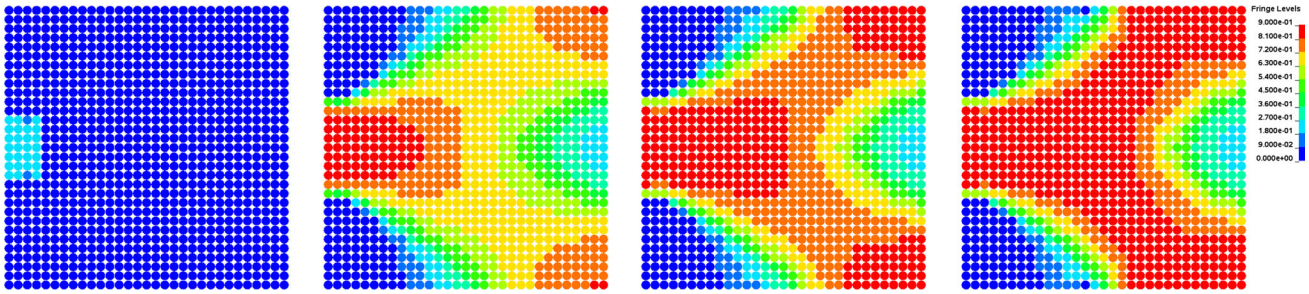

Fig. 10 Damage history in 30 × 30 elements model

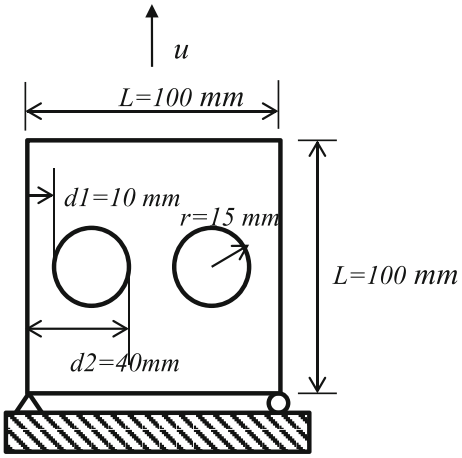

Fig. 11 The problem statement of double-hole model

logical mesh-dependence is exhibited in the finite element solution. The finite element mesh-dependent results can also be detected in their comparison of damage contour shown in Fig. 8a–c. On the other hand, the reaction force response as depicted in Fig. 7b shows the discretization insensitivity of the present method. This discretization insensitivity can be further demonstrated in the results of damage distribution. As shown in Fig. 9a–c, the damage is localized into a zone with a finite width which does not contract as model is continuously refined. The progressive damage contours of the present method are presented in Fig 10. The results in Figs. 8 and 9 indicate that the present method is able to provide the regularization effect for the analysis of elastic-damage induced strain localization problem.

5.3 Double-hole problem

The nonlocal effect of the present method is further investigated in this example by considering the mesh orientation effect. The plate has two holes and is subjected to a displacement control on the top of the surface as shown in Fig. 11. Different from the previous two examples, no geometrical or material imperfections are assumed in this example. The plate has same Young's modulus and Poisson's ratio as in Example 5.2. The damage parameters used in this example are: $\kappa_i = 1.0 \times 10^{-4}$, and $\kappa_c = 1.0 \times 10^{-2}$. Two types of discretization which consists of 4-noded and 3-noded finite elements as displayed in Fig. 12a, b, respectively, are con-

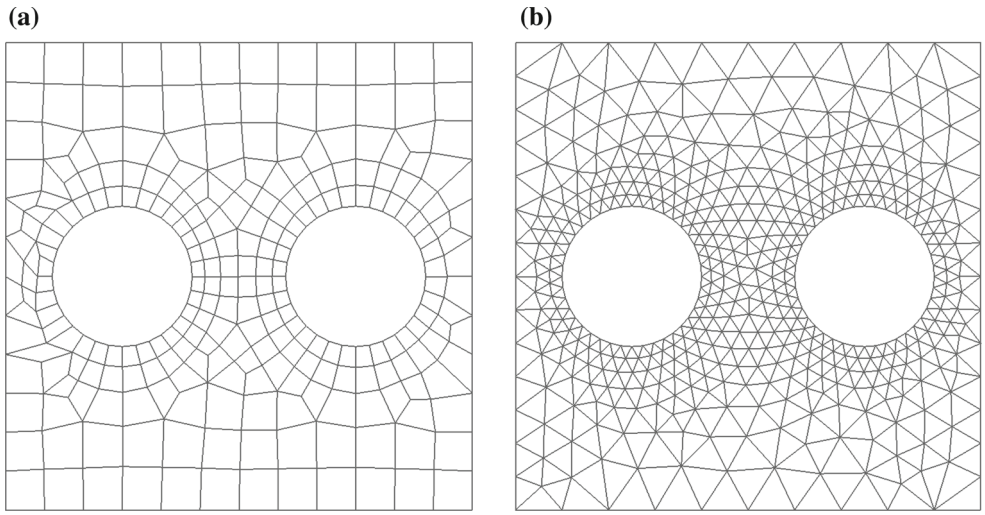

Fig. 12 Two types of discretization in the double-hole problem. **a** 260 4-noded elements, **b** 870 3-noded elements

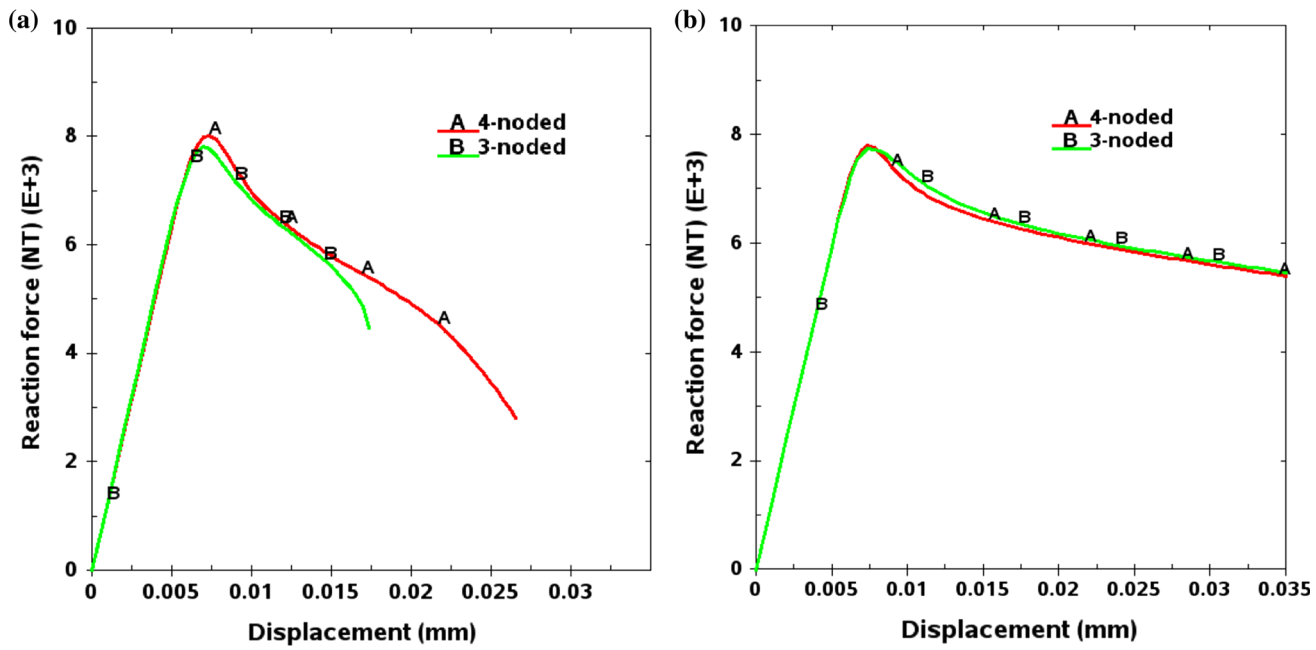

Fig. 13 The force–displacement curves. **a** FEM, **b** present method

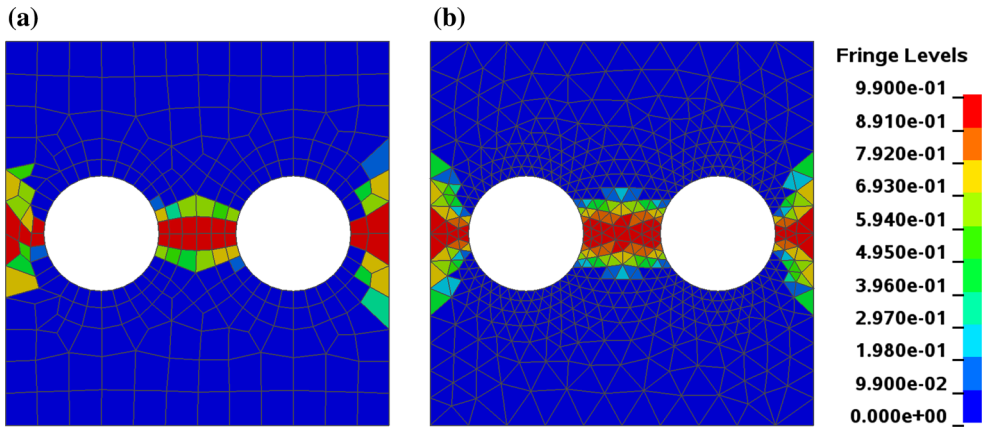

Fig. 14 Comparison of damage contour in FEM. **a** 4-Noded element model, **b** 3-noded element model elements

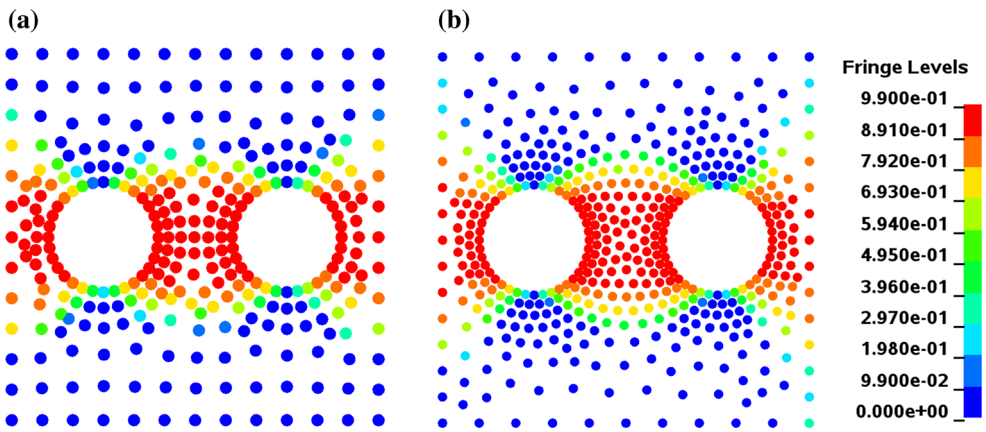

Fig. 15 Comparison of damage contour in present method. **a** 4-Noded element model, **b** 3-noded element model

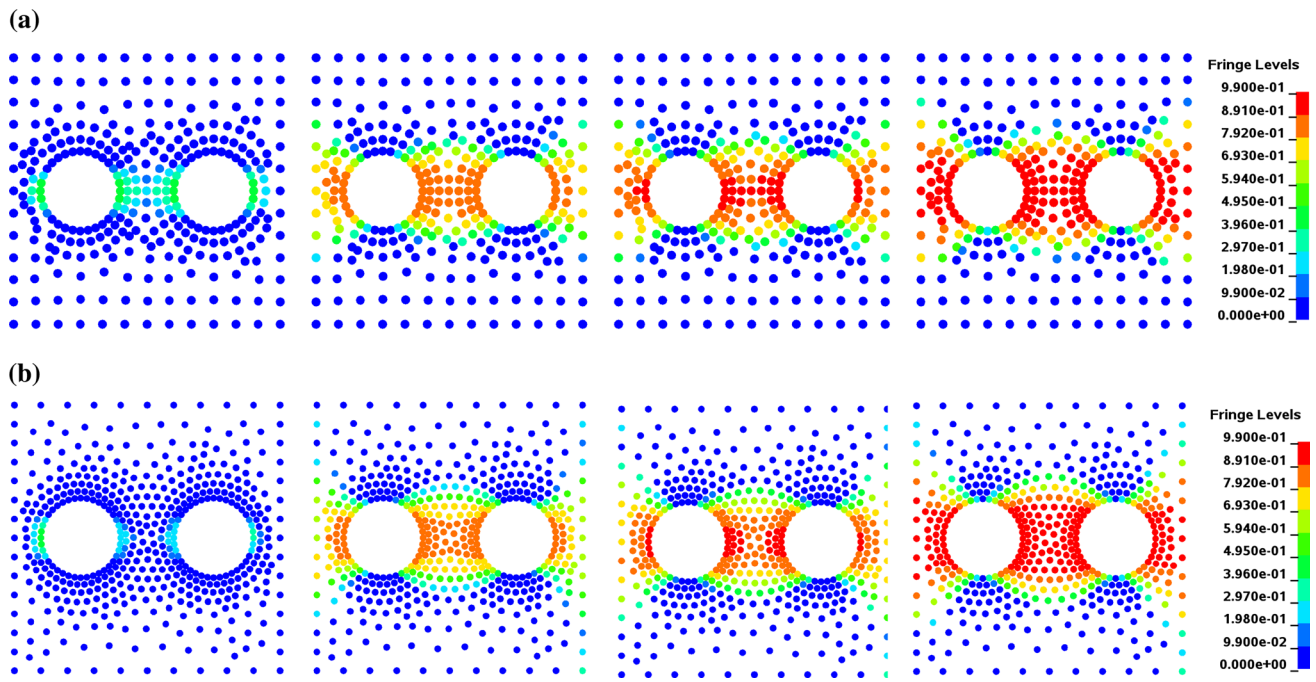

Fig. 16 Damage history. **a** 4-Noded element model, **b** 3-noded element model

sidered in the analysis. In addition to the difference in mesh orientation, the mesh density in Fig. 12a is coarser than that in Fig. 12b near the double-hole area. In the present method, the radius size c of $\tilde{\Psi}^c(\mathbf{x})$ for regularization is taken to be 15 mm for both discretization models.

Figure 13a compares the reaction force response using two different meshes in finite element method. Apparently, strong mesh dependency is observed in the finite element solution in which the mesh orientation and mesh size play a role in affecting the post-damage behavior. Figure 14a, b compare the damage contour at the final deformation for 4-noded and 3-noded mesh, respectively. Both types of finite element discretization generate the localized solutions where the damaged zones form differently in terms of size and pattern.

The comparison of reaction force response using the present method is shown in Fig. 13b which shows a good agreement using two different discretization models. Figures 15a, b present the damage contour displayed in 4-noded and 3-noded finite element discretization, respectively. As shown in Figs. 15a, b, the pattern and size of the damaged zone are comparable in both discretization models. The formation of damage is given in Fig. 16a, b for 4-noded and 3-noded meshes, respectively. The analysis result in this example indicates a regularized and discretization insensitive solution can be achieved by the present method.

6 Conclusions

Similar to the finite element method, the Galerkin meshfree method suffers from a loss of material stability known as the strain localization problem which admits a non-trivial solution and requires regularization. Existing regularized meshfree methods utilizing either integral-type or gradient-type nonlocal damage model encounter intrinsic implementation difficulties when the spatial domain integration is based on the background cells and Gaussian quadrature rule. Additionally, numerical difficulty may also arise when the local and nonlocal strain fields are simultaneously present in the discretization model. This paper presents a strain-morphed nonlocal meshfree method that bypasses the numerical obstacles in the background cells approach while obtains a regularized solution for the analysis of elastic-damage induced strain localization problem.

Three numerical benchmarks are studied to examine the effectiveness of the present approach. The numerical results in this study suggest that the present approach is able to deliver a stable and discretization-objective solution in the analysis of elastic-damage materials. In particular, the size and the pattern of the damage zone in different discretization models are in good agreements throughout the simulation. The application of the method to three-dimensional problem is straight forward and the inclusion of elasti-c-plastic-damage materials is under investigation. The extension of the

present method to the three-dimensional explicit dynamics analysis as well as the coupled damage and fracture analysis will also be considered and presented in the future.

Acknowledgments The authors would like to thank Dr. John O. Hallquist of LSTC for his support to this research. The support from Yokohama Rubber Co. Ltd. to LSTC under the Yosemite Project is greatly acknowledged.

Appendix

We first recall the strain gradient stabilization (SGS) method [37] in linear elasticity analysis where the penalty approach was adopted to introduce the stabilization strain field into the variational formulation. If we assume the homogenous Dirichlet problem for simplicity, the discrete SGS penalty problem [37] in liner elasticity analysis is to find $\hat{\boldsymbol{u}}^p \in V^h \subseteq \boldsymbol{H}_0^1(\Omega)$ such that

$$\overline{\boldsymbol{\Pi}}\left(\hat{\boldsymbol{u}}^p\right) = \inf_{\hat{\boldsymbol{u}} \in V^h} \overline{\boldsymbol{\Pi}}\left(\hat{\boldsymbol{u}}\right) \tag{63}$$

$$\overline{\boldsymbol{\Pi}}\left(\hat{\boldsymbol{u}}\right) = \boldsymbol{\Pi}\left(\hat{\boldsymbol{u}}\right) + \frac{1}{2} s\left(\hat{\boldsymbol{u}}, \hat{\boldsymbol{u}}\right) \tag{64}$$

where

$$\boldsymbol{\Pi}\left(\hat{\boldsymbol{u}}\right) = a^h\left(\hat{\boldsymbol{u}}, \hat{\boldsymbol{u}}\right) + l\left(\hat{\boldsymbol{u}}\right) \tag{65}$$

$$a^h\left(\hat{\boldsymbol{u}}, \hat{\boldsymbol{u}}\right) = \int_\Omega \left(\boldsymbol{\varepsilon}\left(\hat{\boldsymbol{u}}\right)\right)^T : \boldsymbol{C} : \left(\boldsymbol{\varepsilon}\left(\hat{\boldsymbol{u}}\right)\right) d\Omega \tag{66}$$

$$s^h\left(\hat{\boldsymbol{u}}, \hat{\boldsymbol{u}}\right) = \int_\Omega \left(\nabla \boldsymbol{\varepsilon}\left(\hat{\boldsymbol{u}}\right) \cdot \boldsymbol{\lambda}^b\right)^T : \boldsymbol{C} : \left(\nabla \boldsymbol{\varepsilon}\left(\hat{\boldsymbol{u}}\right) \cdot \boldsymbol{\lambda}^b\right) d\Omega \tag{67}$$

The term $l\left(\hat{\boldsymbol{u}}\right)$ in Eq. (65) is the standard external work. The subspace $\boldsymbol{V}^h$ is defined by

$$V^h(\Omega) = \left\{ \boldsymbol{v} : \boldsymbol{v}\Big|_\Omega \in \boldsymbol{H}^1(\Omega), v = \boldsymbol{0} \text{ on } \partial\Omega \right\} \tag{68}$$

For a particle distribution noted by an index set $Z_I = \{\mathbf{x}_I\}_{I=1}^{NP}$, we approximate the displacement field using the meshfree approximation to give

$$\boldsymbol{u}^h(\mathbf{x}) = \sum_{I=1}^{NP} \phi_I^a(\mathbf{x})\, \tilde{\boldsymbol{u}}_I \equiv \hat{\boldsymbol{u}}(\mathbf{x}) \;\; \forall \mathbf{x} \in \Omega \tag{69}$$

where NP is the total number of particles in discretization. $\phi_I^a(\mathbf{x})$, $I = 1, \ldots NP$ can be considered as the shape functions of the meshfree approximation for displacement field $\boldsymbol{u}^h(\mathbf{x})$. Note that the radius size a of $\phi_I^a(\mathbf{X})$ is a numerical length parameter in meshfree displacement approximation and usually $a \neq b$ (for stabilization) $\neq c$ (for regularization). In general, $\tilde{\boldsymbol{u}}_I$ is not the physical particle displacement and is often referred to as the "generalized displacement" [7] of particle I in Galerkin meshfree method. As a result, special essential boundary condition treatment is needed [4]. To simplify the enforcement of essential boundary condition in this study, a first-order meshfree convex approximation [27,31,32] is considered. They are constructed by the Generalized Meshfree Approximation (GMF) method (see [33] for detail mathematical derivation and [34] for the formulations in solid mechanics applications). With the meshfree convex approximation, we can define the $\boldsymbol{H}_0^1$-conforming subspace for the approximation of displacement field to be

$$V^h := span\left\{ \phi_I^a \;\middle|\; \left(supp\ \phi_I^a\right)^0 \subset \Omega,\ I \in Z_I \right\} \tag{70}$$

Since the stabilization coefficient $\boldsymbol{\lambda}^b$ has the property, $\left|\boldsymbol{\lambda}^b(\mathbf{x})\right| \propto h$, where h denotes the size of nodal spacing in meshfree discretization, the solution of Eq. (67) is subjected to a $O\left(h^2\right)$ penalty error [37].

References

1. Bažant ZP, Belytschko T, Chang TP (1984) Continuum theory for strain soften. J Eng Mech 110:1666–1692
2. Bažant ZP, Planas J (1998) Fracture and size effect in concrete and other quasibrittle materials. CRC Press, Boca Raton
3. Beissel S, Belytschko T (1996) Nodal integration of the element-free Galerkin method. Comput Methods Appl Mech Eng 139:49–74
4. Belytschko T, Lu YY, Gu L (1994) Element-free Galerkin methods. Int J Numer Methods Eng 37:229–256
5. Belytschko T, Guo Y, Liu WK, Xiao SP (2000) A unified stability analysis of meshless particle methods. Int J Numer Methods Eng 48:1359–1400
6. Cardoso RPR, Yoon JW, CrJcio JJ, Barlat F (2002) J.M.A. C.M.A. atrd, Development of a one point quadrature shell element for nonlinear applications with contact and anisotropy. Comput Methods Appl Mech Eng 191:5177–5206
7. Chen JS, Pan C, Wu CT, Liu WK (1996) Reproducing kernel particle methods for large deformation analysis of non-linear structures. Comput Methods Appl Mech Eng 139:195–227
8. Chen JS, Wu CT, Belytschko T (2000) Regularization of material instabilities by meshfree approximations with intrinsic length scales. Int J Numer Methods Eng 47:1303–1322
9. Chen JS, Wu CT, Yoon S, You Y (2001) A stabilized conforming nodal integration for Galerkin meshfree methods. Int J Numer Methods Eng 50:435–466
10. Chen JS, Zhang X, Belytschko T (2004) An implicit gradient model by a reproducing kernel strain regularization in strain localization problems. Comput Methods Appl Mech Eng 193:2827–2844
11. Chen JS, Hillman M, Rüter M (2013) An arbitrary order variationally consistent integration for Galerkin Meshfree methods. Int J Numer Methods Eng 95:361–450
12. de Borst R, Muhlhaus HB (1992) Gradient-dependent plasticity: formulation and algorithm aspects. Int J Numer Methods Eng 35:521–539
13. Dyka CT, Randles PW, Ingel RP (1997) Stress points for tension instability in SPH. Int J Numer Methods Eng 40(1997):2325–2341

14. Hillman M, Chen JS, Chi SW (2014) Stabilized and variationally consistent nodal integration for meshfree modeling of impact problems. Comput Part Mech 1:245–256
15. Hill R (1962) Acceleration waves in solids. J Mech Phys Solids 10:1–16
16. Hill R (1958) General theory of uniqueness and stability in elastic–plastic solids. J Mech Phys Solids 6:236–249
17. Lasry D, Belytschko T (1988) Localization limiters in transient problems. Int J Solids Struct 23:581–597
18. Li S, Liu WK (2000) Numerical simulations of strain localization in inelastic solids using mesh-free methods. Int J Numer Methods Eng 48:1285–1309
19. Li S, Liu WK (2004) Meshfree particle method. Springer, Berlin
20. Lian YP, Yang PF, Zhang X, Zhang F, Liu Y, Huang P (2015) A mesh-grading material point method and its parallelization for problems with localized extreme deformation. Comput Methods Appl Mech Eng 289:291–315
21. Lian YP, Zhang X, Zhang F, Cui XX (2014) Tied interface grid material point method for problems with localized extreme deformation. Int J Impact Eng 70:50–61
22. Liu WK, Jun S, Zhang YF (1995) Reproducing kernel particle methods. Int J Numer Methods Fluids 20:1081–1106
23. Peerlings RHJ, de Borst R, Brekelmans WAM, Geers MGD (2002) Localization issues in local and nonlocal continuum approaches to fracture. Eur J Mech A 21:175–189
24. Rabczuk T, Belytschko T, Xiao SP (2004) Stable particle methods based on Lagrangian kernels. Comput Methods Appl Mech Eng 193:1035–1063
25. Silling SA, Askari E (2005) A meshfree method based on the peridynamic model of solid mechanics. Comput Struct 83:1526–1535
26. Simo JC, Hughes TJR (1986) On the variational foundation of assumed strain methods. ASME J Appl Mech 53:51–54
27. Sukumar N (2004) Construction of polygonal interpolants: a maximum entropy approach. Int J Numer Methods Eng 61:2159–2181
28. Wang DD, Peng H (2013) A Hermite reproducing kernel Galerkin meshfree approach for buckling analysis on thin plates. Comput Mech 51:1013–1029
29. Wang DD, Li Z (2013) A two-level strain smoothing regularized meshfree approach with stabilized conforming nodal integration for elastic damage analysis. Int J Damage Mech 22:440–459
30. Wang DD, Li L, Li Z (2014) A regularized Lagrangian meshfree method for rainfall infiltration triggered slope failure analysis. Eng Anal Bound Elem 42:51–59
31. Wang DD, Chen P (2014) Quasi-convex reproducing kernel meshfree method. Comput Mech 54:689–709
32. Wu CT, Koishi M (2009) A meshfree procedure for the microscopic analysis of particle-reinforced rubber compounds. Interact Multiscale Mech 2:147–169
33. Wu CT, Park CK, Chen JS (2011) A generalized approximation for the meshfree analysis of solids. Int J Numer Methods Eng 85:693–722
34. Wu CT, Guo Y, Askari E (2013) Numerical modeling of composite solids using an immersed meshfree Galerkin method. Compos Part B 45:1397–1413
35. Wu CT, Guo Y, Hu W (2014) An introduction to the LS-DYNA smoothed particle Galerkin method for severe deformation and failure analysis in solids. In: 13th international LS-DYNA users conference, Detroit. 8–10 June, pp 1–20
36. Wu CT, Ren B (2015) A stabilized non-ordinary state-based peridynamics for the nonlocal ductile material failure analysis in metal machining process. Comput Methods Appl Mech Eng 291:197–215
37. Wu CT, Koishi M, Hu W (2015) A displacement smoothing induced strain gradient stabilization for the meshfree Galerkin nodal integration method. Comput Mech 56:19–37
38. Wu YC, Wang DD, Wu CT (2014) Three dimensional fragmentation simulation of concrete structures with a nodally regularized meshfree method. Theor Appl Fract Mech 27:89–99
39. Wu YC, Wang DD, Wu CT (2015) A direct displacement smoothing meshfree particle formulation for impact failure modeling. Int J Impact Eng. doi:10.1016/j.ijimpeng.2015.03.013